Toxicology Letters 211 (2012) 334–341

Contents lists available at SciVerse ScienceDirect

Toxicology Letters

journal homepage: www.elsevier.com/locate/toxlet

Silver nanoparticles-mediated G2/M cycle arrest of renal epithelial cells is associated with NRF2-GSH signaling

Su Jin Kang[a], Young Joon Lee[a], Eun-Kyung Lee[b], Mi-Kyoung Kwak[c,*]

[a] Daegu Haany University, College of Oriental Medicine, Gyeongsan-si, Gyeongsangbuk-do 712-715, Republic of Korea
[b] Yeungnam University, College of Pharmacy, Gyeongsan-si, Gyeongsangbuk-do 712-749, Republic of Korea
[c] The Catholic University of Korea, College of Pharmacy, 43 Jibong-ro, Wonmi-gu, Bucheon, Gyeonggi-do 420-743, Republic of Korea

ARTICLE INFO

Article history:
Received 28 February 2012
Received in revised form 18 April 2012
Accepted 20 April 2012
Available online 28 April 2012

Keywords:
Silver nanoparticles
NRF2
Renal epithelial cells
GSH
G2/M arrest

ABSTRACT

Silver nanoparticles (nAg) are known to evoke reactive oxygen species (ROS) generation and consequent cell damage. The transcription factor NF-E2-related factor 2 (NRF2) controls both the basal and inducible expression of multiple antioxidant genes. This study was aimed to investigate the role of NRF2 in nAg-induced renal epithelial cell damage. nAg treatment intensified DNA damage and G2/M cell cycle arrest by nAg in *NRF2* knockdown HK-2 (NRF2i) compared with the control cells. As a signaling mechanism associated with nAg-mediated growth arrest, the levels of phospho-CDC25C and phospho-CDC2 were significantly increased in NRF2i. Target gene analysis revealed that nAg-mediated increase in γ-glutamate cysteine ligase expression is NRF2-dependent: nAg-treated NRF2i showed a reduction in glutathione (GSH) content and elevation in ROS level in comparison with the control cells. Additionally, pretreatment of *N*-acetylcystein in nAg-treated NRF2i alleviated ROS-mediated DNA damage and G2/M cell cycle arrest, while GSH depletion exacerbated DNA damage and cell cycle arrest in the control cells. Taken together, these results suggest that NRF2-mediated GSH increase plays a protective role in nAg-induced DNA damage and subsequent G2/M cell cycle arrest in human renal epithelial cells.

1. Introduction

Silver nanoparticles (nAg), one of the most well-known nanomaterials, have been widely used in various commercial products including electric home appliances and infant products due to their strong anti-bacterial activity (Cohen et al., 2007; Sondi and Salopek-Sondi, 2004). In particular, medical products including nAg-wound dressing and nAg-coated implantable devices are currently available (Chaloupka et al., 2010). Although human exposure to nAg is rapidly increasing, little is known about the potential risk to human health. On account of small size, nanoparticles can be distributed in subepithelial space to a greater extent than larger particles (Churg et al., 1998). Several studies have reported that nano-scale particles such as nAg can be translocated from the lungs into the blood (Donaldson et al., 2001; Loeschner et al., 2011; Nemmar et al., 2001; Tang et al., 2009), and can thereby move to other organs including heart, liver and kidney (Kim et al., 2010; Samet et al., 2004). Accumulating evidence suggests that nAg evoke intracellular production of reactive oxygen species (ROS) in different types of cells (Piao et al., 2011; Yoshimaru et al., 2006). nAg induce oxidative cell damage in human liver cells through the suppression of reduced GSH level and the induction of mitochondria-involved apoptosis (Piao et al., 2011). In addition, nAg suppress cell cycle progression due to their DNA damaging property (AshaRani et al., 2009; Eom and Choi, 2010).

When ROS production is increased above the normal level, the nuclear factor NF-E2-related factor 2 (NRF2) activates the expression of an array of antioxidant genes, resulting in the protection of cells from oxidative insults. NRF2-regulated genes include a subset of genes encoding phase II detoxifying enzymes (*e.g.*, NAD(P)H quinone oxidoreductase-1 [NQO1]), thiol-containing systems (*e.g.*, γ-glutamate cysteine ligase [GCL]), direct ROS removing enzymes (*e.g.*, GSH peroxidase [GPX]), and stress-response proteins (*e.g.*, heme oxygenase-1 [HO-1]) (Hayes et al., 2010; Kensler et al., 2007; Kobayashi and Yamamoto, 2005; Kwak and Kensler, 2010). Glutathione (GSH) is a major cellular thiol antioxidant and a co-substrate for many antioxidant and representative phase II

Abbreviations: nAg, silver nanoparticle; NRF2i, NRF2 knockdown HK-2; SCi, nonspecific control HK-2; scRNA, scrambled RNA; ARE, antioxidant-response element; ROS, reactive oxygen species; GSH, glutathione; NQO1, NAP(D)H:quinone oxidoreductase-1; GCLC, catalytic subunit of γ-glutamate cysteine ligase; GCLM, modulatory subunits of γ-glutamate cysteine ligase; HO-1, heme oxygenase-1; MT, metallothionein; HSP, heat shock protein; SOD, superoxide dismutase; GPX, glutathione peroxidase; MTT, 3-(4,5-dimethylthiazol-2-yl)-2,5-diphenyltetrazolium bromide; NAC, *N*-acetylcysteine; BSO, L-buthionine-[S,R]- sulfoximine; PI, propidium iodide; MN, micronuclei; NDI, nuclear division index; CDC, cell division cycle; CDK, cyclin-dependent kinase.

* Corresponding author. Tel.: +82 2 2164 6532; fax: +82 2 2164 4059.
E-mail address: mkwak@catholic.ac.kr (M.-K. Kwak).

0378-4274/$ – see front matter © 2012 Elsevier Ireland Ltd. All rights reserved.
http://dx.doi.org/10.1016/j.toxlet.2012.04.016

enzymes. Diminution in GSH content affects cellular redox status and also likely leads to an increased susceptibility to a variety of environmental stress (Harvey et al., 2009). Therefore, the induction of enzymes required for its synthesis is one of key adaptive responses to oxidative stress. GSH is synthesized from its constituent amino acids by two ATP-dependent enzymes: GCL and GSH synthetase (GSS). GCL, the rate-limiting enzyme, is a heterodimer composed of GCLC (the catalytic subunit of GCL) and GCLM (the mosulatory subunit of GCL), and the expression of these enzymes are under the control of NRF2 (Liu and Choi, 2000; Uejima et al., 1993).

This study was aimed to investigate the potential cytotoxicity of nAg in human renal epithelial cells, and the role of NRF2 in nAg toxicity has been elucidated. For this purpose, we have established *NRF2* knockdown stable proximal epithelial HK-2 cells. As a result, the genetic inhibition of *NRF2* in these cells intensified nAg-mediated DNA damage and G2/M cell growth arrest by suppressing GSH increase and thereby increasing ROS production.

2. Materials and methods

2.1. Materials

nAg (NANOMIX™-PS53) was purchased from NanoPoly Co. Ltd. (Seoul, Korea) (Hwang et al., 2008; Kang et al., 2012; Kim et al., 2009). This product is a transparent water-based nAg colloid form (pH 6–8) with 7.5 ± 2.5 nm particle size. Manufacturer's provided information verified that nAg product contains metallic nAg, which was confirmed by the Thermogravimetry-Differential Thermal Analysis. 3-(4,5-Dimethylthiazol-2-yl)-2, 5-diphenyltetrazolium bromide (MTT) was purchased from Amresco Inc. (Solon, Ohio, USA). *N*-Acetylcysteine (NAC), L-buthionine-[S,R]-sulfoximine (BSO), and cytochalasin-B were purchased from Sigma–Aldrich (Saint Louis, MO, USA). Antibodies against phospho-cell division cycle 25C (CDC25C; Ser216), cyclin-dependent kinase 2 (CDK2), cycline E1, and cycline B1 were obtained from Cell Signaling Technology (Beverly, MA, USA). Antibodies recognizing p53, p21, p27, phospho-CDC2 (Tyr15), CDC2, CDC25C and β-tubulin were obtained from Santa Cruz Biotechnology (Santa Cruz, CA, USA). The lentiviral expression plasmids for NRF2 shRNA, Mission™ Lentiviral Packing Mix, hexadimethrine bromide and puromycin were obtained from Sigma–Aldrich.

2.2. Cell culture

HK-2 (human renal proximal tubular epithelial cells) was purchased from American Type Culture Collection (Manassas, VA, USA) and maintained in DME/F-12 (1:1) (HyClone) containing 10% fetal bovine serum and penicillin/streptomycin (HyClone). Cells were maintained at 37 °C under an atmosphere of 5% CO_2.

2.3. Production of shRNA lentiviral particles and establishment of stable cell lines

Establishment of NRF2 knockdown HK-2 was performed as described previously (Kim et al., 2011). Briefly, HEK 293T cells were transfected with 1.5 μg pLKO.1-NRF2 shRNA and the Packaging Mix using a Lipofectamine 2000 (Invitrogen, Carlsbad, CA, USA). Nonspecific scrambled RNA (scRNA) expressing pLKO.1-scRNA plasmid was used for the production of nonspecific control shRNA. Media containing lentiviral particles were collected and used for a stable transduction of HK-2 cells with puromycin selection for up to 4 weeks.

2.4. MTT assay

Viable cell number was determined using the MTT assay. Briefly, cells were seeded at a density of 5×10^3 cells/well in 96-well plates. After the incubation of cells with nAg (5 μg/ml, 15 μg/ml, 30 μg/ml, or 60 μg/ml) for 0 h, 12 h, 24 h or 48 h, MTT solution (2 mg/ml) was added and plates were further incubated for 4 h. Following the removal of MTT solution, 100 μl of DMSO was added to each well and absorbance was measured at 540 nm using a Versamax microplate reader (Sunnyvale, CA, USA).

2.5. Cytokinesis-block micronucleus assay

The cytokinesis-block micronucleus (CBMN) assay was performed as described by Fenech (2000). After nAg treatment in HK-2 cells, cytochalasin-B (4 μg/ml) was added and the incubation was continued for an additional 28 h. Cells were harvested and treated twice with 0.075 M of KCl hypotonic solution for 1 min. Then, a fixation solution (a mixture of methanol (3) and acetic acid (1)) was added and cell preparations were stained with Giemsa solution (5%). The frequency of micronuclei (MN) was assessed by measuring binucleated cells with well-preserved cytoplasm (Fenech, 2000). The nuclear division index (NDI) was evaluated in 500 cells from each sample to determine the percentage of cells with mono-, bi-, and multi-nuclei. The NDI was calculated by using the standard formula (Eastmond and Tucker, 1989).

2.6. Flow cytometric analysis of cell cycle

Cells were cultured in 6-well plates and treated with nAg (30 μg/ml or 60 μg/ml). After the treatment, cells were fixed in 70% ethanol at least for 4 h and permeabilized with 0.1% Triton X-100. Then, cells were stained with 20 μg/ml propidium iodide (PI; Sigma–Aldrich) solution containing 100 μg/ml RNase A (Sigma–Aldrich) for 20 min at 37 °C. Cell populations under G0/G1, S and G2/M phase among 10,000 cells were determined by employing regions with FL2 area *vs* FL2 width. Analysis was done by a flow cytometry (FACSCalibur, BD Bioscience, NJ, USA) and CellQuest software (BD Bioscience) using histogram statistics for cell cycle.

2.7. Western blot analysis

Cells were lyzed with RIPA buffer (50 mM Tris (pH 7.4), 150 mM NaCl, 1 mM EDTA, and 1% NP40) containing protease inhibitor cocktail (Sigma–Aldrich). Protein concentration was determined using a DC protein assay kit (Bio-Rad, Hercules, CA, USA). Protein samples were separated by electrophoresis on 10–12% SDS-polyacrylamide gels and transferred to nitrocellulose membranes (Whatman GmbH, Dassel, Germany) using a Trans-Blot® Semi-Dry Cell (Bio-Rad). The membrane was then blocked with 3% skim milk for 1 h, and incubated with first and secondary antibodies. Chemiluminescent detection was done using a Fujifilm LAS-4000 mini (Fujifilm, Tokyo, Japan).

2.8. Total RNA extraction and RT-PCR analysis

Total RNAs were isolated from cells using a TRIzol reagent (Invitrogen, Carlsbad, CA, USA) following the treatment of cells with nAg for 24 h. Synthesis of cDNAs was performed by a reverse transcriptase (RT) reaction and a real time RT-PCR analysis was performed with a Roche LightCycler (Mannheim, Germany) using the Takara SYBR Premix ExTaq system (Otsu, Japan). Primers were synthesized by Bioneer (Daejeon, South Korea) and primer sequences for human genes are: GCLC, 5′-ATGATGCCAACGAGTCTGAC-3′ and 5′-CGCCTTTGCAGATGTCTTTC-3′; GCLM, 5′-AGGAGCTTCGGGACTGTATT-3′ and 5′-TGGGCTTCAATGTCAGGGAT-3′; NQO1, 5′-CAGTGGTTTGGAGTCCCTGCC-3′ and 5′-TCCCCGTGGATCCCTTGCAG-3′; HO-1, 5′-GCTGCTGACCCATGACACCAAGG-3′ and 5′-AAGGACCCATCGGAGAAGCG-GAG-3′; NRF2, 5′-ATAGCTGAGCCCAGTATC-3′ and 5′-CATGCACGTGAGTGC-TCT-3′; superoxide dismutase 1 (SOD1), 5′-GATTCCATGTTCATGAGTTT-3′ and 5′-AGGATAACAGATGAGTTAAG-3′; SOD2, 5′-AACCTCACATCAACGCGCAGAT-3′ and 5′-TCAGTGCAGGCTGAAGAGCTAT-3′; metallothionein 1A (MT1A), 5′-CCTTCCACGTGCGCCTTATAGC-3′ and 5′-ACACTTGGCACAGCTCATGGG-3′; MT2A, 5′-TGGACCCCAACTGCTCCTGT-3′ and 5′-AGCTGCACTTGTCCGAAGCC-3′; heat shock protein 70 (HSP70), 5′-GTGGACCAGGAGGAACCACATG-3′ and 5′-ATTGGCAGGTCCACAGTACTGG-3′; HSP90, 5′-GCAACAGCCACAGACACCAGCA-3′ and 5′-TCAATGGGCAGGTCCACGGT-3′; GPX1, 5′-GATGAACGATCTGCAGAAGC-3′ and 5′-CAAAGTTCCAGGCAATGTCG-3′; GPX2, 5′-TCATGACCGATCCCAAGCTCAT-3′ and 5′-ATGGCAACTTTAAGGAGGCGCT-3′; hypoxanthine-guanine phosphoribosyltransferase (HPRT), 5′-TGGCGTCGTGATTAGTGATG-3′ and 5′-GCTACAATGTGATGGCCTCC-3′.

2.9. Measurement of total GSH contents

Cells were grown in 6-well plates and treated with nAg for 48 h and lysed with 5% metaphosphoric acid solution. For measuring total GSH content, optical densities were monitored for 4 min following an incubation of 30 μl cell lysates with 30 μl 5, 5-dithiobis (2-nitrobenzoic acid), glutathione reductase and β-NADPH. Protein concentration was determined by BCA protein assay kit (Pierce, IL, USA).

2.10. Measurement of ROS production

Cellular ROS levels were determined using a fluorogenic probe 5-(and-6)-carboxy-2′,7′-dichlorodihydrofluorescein diacetate (carboxy-H_2DCFDA). Cells in 96-well plates were incubated with 25 μM carboxy-H_2DCFDA for 30 min at 37 °C. After the incubation, cells were washed with PBS and fluorescent intensities were determined using a Fluorostar Optima (BMG Labtech, Ortenberg, Germany) at excitation 485 nm/emission 520 nm.

2.11. Statistical analyses

All experiments were performed in at least two replicates and three to four individual experiments were carried out. Statistical significance was determined by Student *t*-test or one-way ANOVA followed by Student-Newman–Keuls's comparison method using SPSS 11 (SPSS Inc., Chicago, IL, USA).

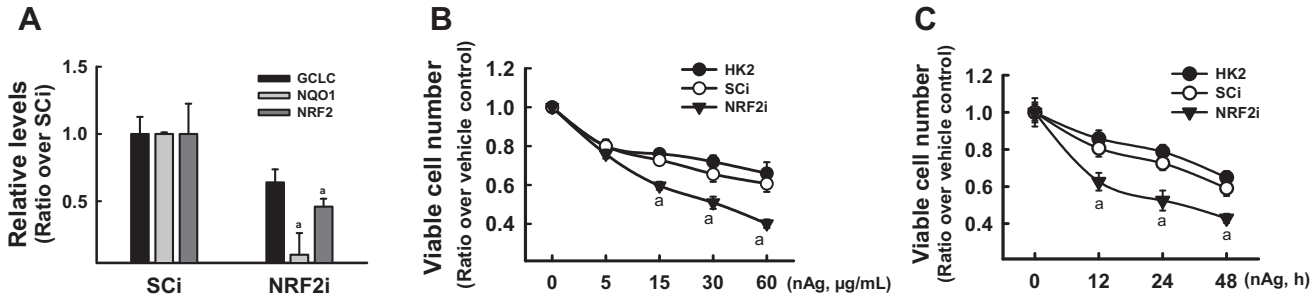

Fig. 1. Establishment of NRF2i and the suppression of viable cell number by nAg. (A) HK-2 cells were transduced by lentiviral particles containing either a nonspecific control scRNA- or NRF2 shRNA-expressing plasmid and puromycin selection was performed. Inhibition of NRF2 was verified by measuring transcript levels for NRF2, GCLC, and NQO1 in established nonspecific control (SCi) and NRF2-shRNA expressing cells (NRF2i) using a real-time RT-PCR analysis. Values are relative expressions compared to nonspecific SCi control. (B) Viable cell number was determined by the MTT assay in unmodified HK-2, SCi, and NRF2i following treatment with nAg (0, 5, 15, 30, and 60 μg/ml) for 24 h. (C) Viable cell number was monitored following 60 μg/ml nAg for 0, 12, 24, or 48 h. Values are means ± SD from three experiments. [a] $P < 0.05$ compared with nonspecific SCi control.

3. Results

3.1. The decrease of viable cell number is profound in nAg-treated NRF2 knockdown renal epithelial cells

After the stable transduction of HK-2 cells with nonspecific scRNA (SCi) or NRF2 shRNA cells (NRF2i), *NRF2* knockdown was verified by the measurement of NRF2 and its target genes GCLC and NQO1 using a real-time RT-PCR analysis (Fig. 1A). In NRF2i, the expression level of NRF2 decreased by 54% and GCLC level reduced to 64% compared to the nonspecific scRNA transduced control HK-2 (SCi). Then, cells were incubated with varied concentrations of nAg (0, 5, 15, 30, and 60 μg/ml) for 24 h and cytotoxic effect of nAg was tested. First, viable cell number was repressed by 40% following 60 μg/ml nAg in HK-2 cells. This indicates that relatively high concentration of nAg is required to affect the viable cell number of HK-2 compared to other types of cells (Ahamed et al., 2010). It is of note that nAg incubation for 24 h at these concentrations did not cause a significant morphology change representing necrosis or apoptosis. It was apparent that cell number was decreased by nAg in HK-2. Second, the MTT assay in SCi and NRF2i indicates that a viable cell number in NRF2i group was significantly lower compared to the unmodified HK-2 as well as SCi control (Fig. 1B). In the analysis of time-dependence, NRF2i showed significantly greater cytotoxicity following 12, 24, and 48 h incubation of nAg (Fig. 1C). Similarly to HK-2, viable cell number following nAg treatment was significantly reduced in *Nrf2* knockdown rat renal epithelial NRK-52E compared to unmodified and nonspecific scRNA transduced NRK-52E (data not shown).

3.2. NRF2i is more susceptible to nAg-induced DNA damage and cell cycle arrest than SCi

In order to define the reason of reduced cell number after nAg treatment, we have analyzed cell cycle distribution of nAg-treated SCi and NRF2i. After nAg incubation for 48 h, both cell lines exhibited a dose-dependent G2/M arrest (Fig. 2A). However, arrested cell proportion was greater in NRF2i (36%) than that in SCi (25%). It is of note that nAg-mediated growth arrest appears to be associated with oxidative stress: NAC treatment alleviated G2/M arrest by nano-Ag in NRF2i (Fig. 2B).

To assess the linkage between G2/M cell cycle arrest and DNA damage in these cells, we performed CBMN assay. CBMN assay is wildly used to evaluate the DNA damage, chromosome damage and cytostasis following the exposure to chemicals and environmental contaminants (Fenech, 2007; Kang et al., 2008; Kirsch-Volders et al., 2011). First, the MN frequency, which is a biomarker of chromosome damage, was significantly increased by 60 μg/ml nAg only in NRF2i (Fig. 2C). Second, the NDI, which is a measurement of proportion of mono-, bi-, and multi-nucleated cells, is used to monitor cytostatic effect of chemicals (Fenech, 2007). The NDI value was significantly decreased by nAg in both cell lines and the decrease was greater in NRF2i than that in SCi (Fig. 2D). Involvement of oxidative stress in DNA damage and cytostasis was additionally supported by results from NAC treatment: NAC alleviated MN frequency increase and NDI decrease only in NRF2i but not in SCi (Fig. 2C and D). Displayed evidence suggests that *NRF2* knockdown intensifies nAg-mediated DNA damage, cytostasis at G2/M phase, and consequent growth inhibition.

3.3. Components for cell cycle progression were differentially affected by NRF2 knockdown

DNA damage can affect multiple signaling pathways leading to cell growth inhibition. In our cell system, nAg induced G2/M growth arrest, therefore mechanisms involving in this phenomenon has been explored. When components for G2 to M phase progression were analyzed, the increase of phospho-CDC2 (cyclin-dependent kinase 1, CDK1), which is an inactive form of CDC2, was more prominent in NRF2i compared to SCi (Fig. 3A). CDC2 activity can be controlled by multiple pathways, and among them, CDC25 activates CDC2 signaling by acting as a CDC2 phosphatase. We observed that CDC25C is highly phosphorylated in nAg-treated NRF2i, indicating that nAg-mediated DNA damage inhibits CDC25C function and consequently results in G2/M cell cycle arrest. While, nAg decreased Cycline B1 level in both cell lines (Fig. 3A). This implies that enhanced growth arrest shown in NRF2i is associated CDC2 activity. Meanwhile, p53 protein is a core molecule mediating G2/M and G1/S checkpoint activation in response to DNA damage. nAg treatment increased protein level of p53 in NRF2i in a greater extent compared to SCi (Fig. 3B), which is in accord with results of DNA damage index. At the same time, level of p21, a p53-dependent CDK inhibitor, showed a similar pattern: nAg-mediated increase of p21 was higher in NRF2i than that in SCi. Furthermore, level of p27, which is a checkpoint protein for both G1/S and G2/M phases, increased in NRF2i. Although cell populations in G1/S phase were not increased by nAg, component for G1-S progression were also affected: cyclin E1 is elevated by nAg in both cell lines, while CDK2 level is reduced only in NRF2i (Fig. 3C). Taken together, it can be concluded that DNA damage in nAg-treated NRF2i cells may activate G2/M checkpoint by elevating levels of phospho-CDC2 and phospho-CDC25C.

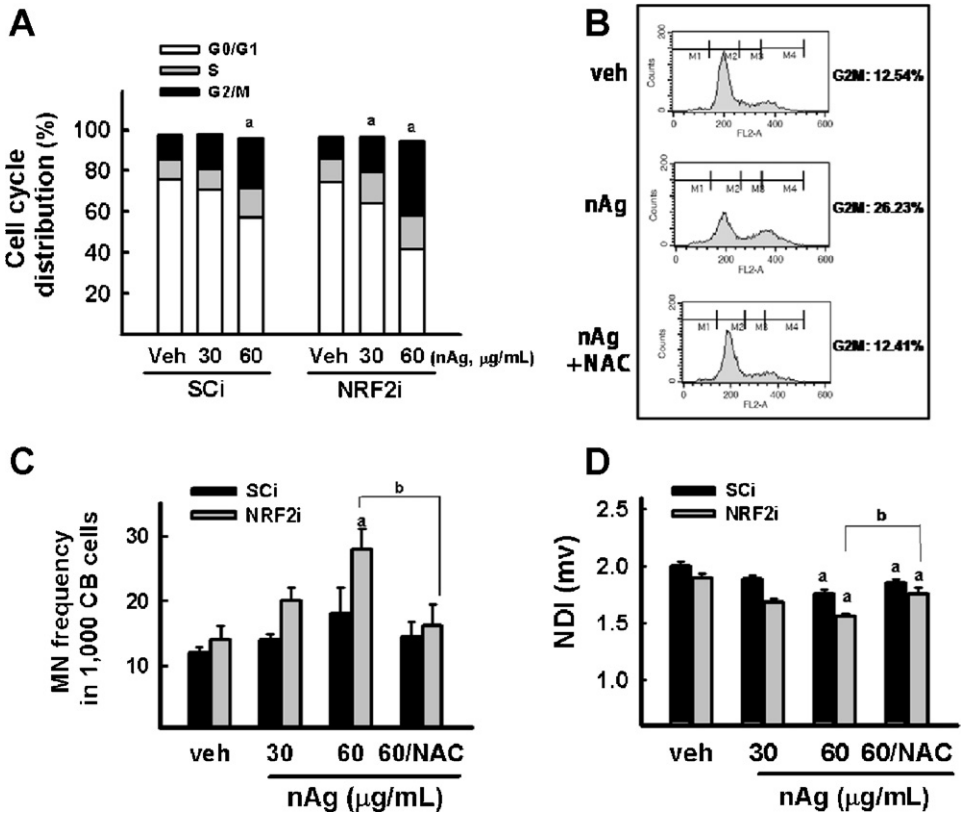

Fig. 2. nAg induce DNA damage and G2/M cell cycle arrest in *NRF2i*. (A) Cell cycle distribution was analyzed by measuring cell fractions in G0/G1, S, and G2/M phase using a fluorescence-activated cell sorter (FACS) analysis. Cells were treated with vehicle (veh, water) or nAg (30 and 60 μg/ml) for 48 h. Values are means ± SD from three experiments. Statistical analysis indicates the comparison of cell fractions in G2/M phase. [a] $P < 0.05$ compared with each vehicle-treated group. (B) In NRF2i, NAC (5 mM) was added 6 h prior to nAg and further incubated for 48 h. Cell cycle distribution was analyzed by FACS. (C) Levels of DNA damage measured by MN frequency were analyzed in SCi and NRF2i following treatment with vehicle (veh, water) or nAg (30 μg/ml or 60 μg/ml) for 48 h. NAC was added 6 h prior to nAg and further incubated for 48 h. (D) The NDI was determined in SCi and NRF2i following vehicle- or nAg (30 μg/ml or 60 μg/ml)-treatment for 48 h. Values are means ± SD from three experiments. [a] $P < 0.05$ compared with each vehicle-treated group. [b] $P < 0.05$ compared with nAg-treated NRF2i cells.

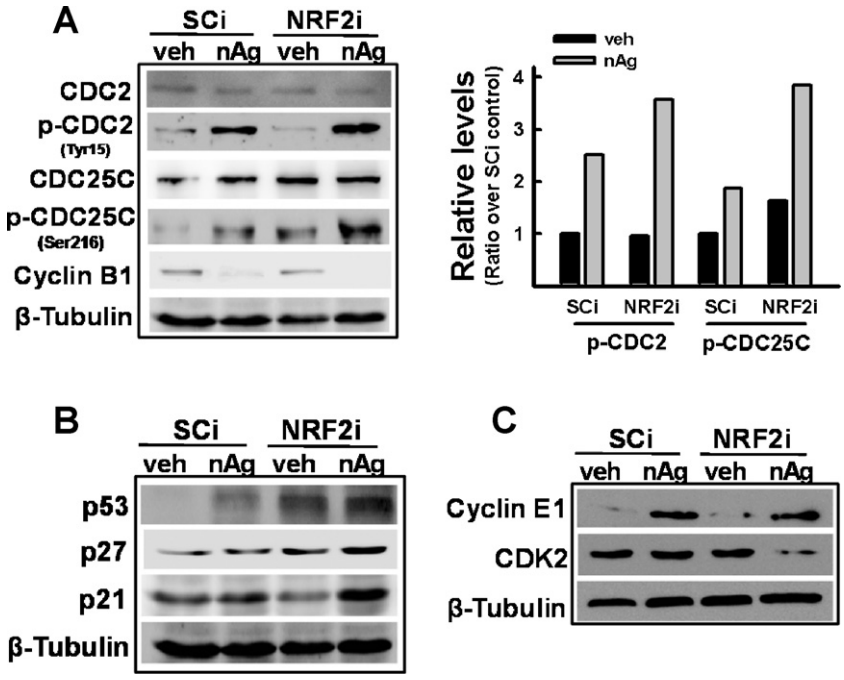

Fig. 3. nAg treatment modulates the levels of cell cycle-associated proteins in an NRF2-dependent manner. (A) Protein levels for CDC2, p-CDC2 (Ser216), CDC25C, p-CDC25C (Tyr15), Cyclin B1, and β-tubulin were analyzed following nAg (60 μg/ml) treatment for 48 h. Bar graph shows relative levels of p-CDC2 and p-CDC25C. (B) Protein levels for p53, p27, p21, and β-tubulin were monitored following vehicle (veh, water) or nAg (60 μg/ml) treatment in SCi and NRF2i. (C) Protein levels for Cyclin E1, CDK2, and β-tubulin were analyzed following nAg treatment. Similar blots were obtained from three different experiments.

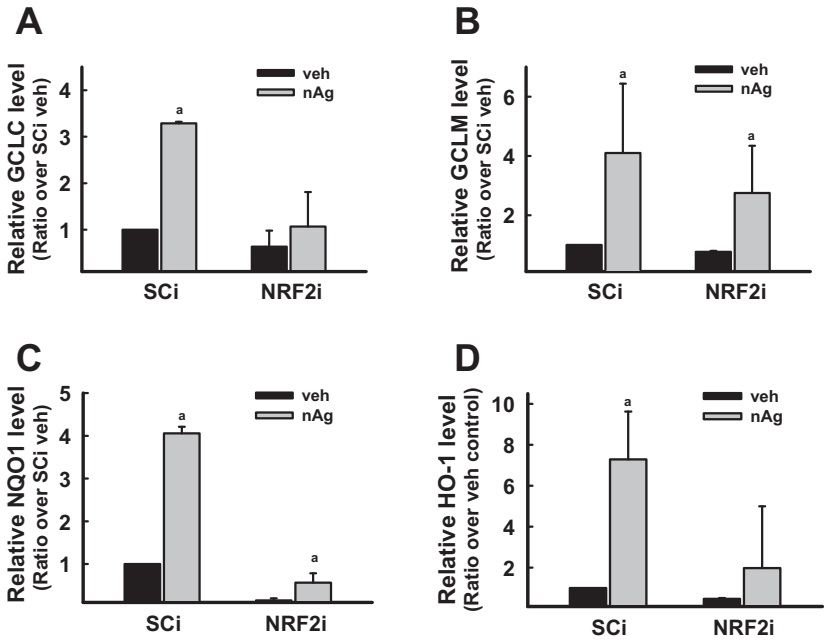

Fig. 4. NRF2-dependent nAg-inducible genes. Transcript levels for GCLC (A), GCLM (B), NQO-1 (C), and HO-1 (D) were measured using a real-time PCR analysis following the treatment of SCi and NRF2i with vehicle (veh, water) or nAg (60 μg/ml) for 24 h. Values are means ± SD from three experiments. [a] $P < 0.05$ compared with vehicle-treated group.

Table 1
Relative levels of gene expression in SCi and NRF2i following vehicle (veh, water) or nAg (60 μg/ml) incubation for 24 h.

Cell line Treatment	SCi veh	SCi nAg	NRF2i veh	NRF2i nAg
MT1A	1 ± 0.02	11.20 ± 5.70	1.27 ± 0.08	7.94 ± 4.00
MT2A	1 ± 0.06	4.95 ± 1.34	0.87 ± 0.14	4.33 ± 0.60
HSP70	1 ± 0.02	1.37 ± 0.31	0.40 ± 0.11	1.40 ± 0.59
HSP90	1 ± 0.04	1.56 ± 0.14	0.69 ± 0.15	1.59 ± 0.53
SOD1	1 ± 0.02	2.96 ± 0.12	0.78 ± 0.03	1.16 ± 0.05
SOD2	1 ± 0.03	0.76 ± 0.23	0.74 ± 0.07	0.34 ± 0.20
GPX1	1 ± 0.04	1.22 ± 0.34	0.98 ± 0.03	0.74 ± 0.30
GPX2	1 ± 0.02	2.74 ± 0.22	0.61 ± 0.5	1.04 ± 0.28

3.4. nAg elevate antioxidant gene expression in an NRF2-dependent manner

In an effort to examine the cause of distinct nAg sensitivity shown in NRF2i, transcript levels for NRF2-target genes were assessed in nAg-treated cells using a real-time PCR analysis. Results indicate that nAg increase the expression of NQO1, HO-1 and GSH synthesis enzymes such as GCLC and GCLM. In particular, these increases were profound in SCi control, while NRF2i showed marginal or insignificant increases (Fig. 4A–D). The metal detoxification related-genes including MT and HSP, and ROS-scavenging genes such as SOD and GPX were also determined (Table 1). nAg treatment could elevate levels for these metal-detoxification and ROS scavenging genes: (i) MT1A and MT1B were elevated in both SCi and NRF2i, (ii) HSP70 and HSP90 expression was only marginally affected by nAg, (iii) SOD1 level was elevated by nAg only in SCi, and (iv) GPX2 increase was only observed in SCi. These suggest that differential expression of NRF2-target genes may be responsible for the distinct sensitivity of NRF2i to nAg.

3.5. GSH is a key factor determining nAg cytotoxicity in renal epithelial cells

In order to clarify the role of NRF2-mediated GCLC increase in cell survival, we determined the levels of GSH and ROS after nAg treatment. First, nAg increased total cellular GSH by 2.5-fold in SCi, while no increase was observed in NRF2i (Fig. 5A). Second, cellular ROS level increase was higher in NRF2i than that in SCi (Fig. 5B). These imply that NRF2 inhibition suppresses nAg-mediated GCLC induction, which results in a failure of GSH increase. In fact, treatment with NAC completely prevented ROS increase in NRF2i.

Next, the effect of pharmacological inhibitor of GSH on nAg has been investigated. BSO is a selective and irreversible inhibitor of GCL, and the incubation of HK-2 cells with 10 μM BSO for 24 h could deplete total GSH by up to 93% (data not shown). In SCi, BSO pre-treatment significantly aggravated nAg-mediated cell number repression, DNA damage, and cytostasis, while NRF2i did not show notable changes upon BSO treatment (Fig. 6A–C). Cell cycle arrest at G2/M phase was also intensified by BSO treatment (Fig. 6D). These indicate that NRF2-meidated GSH increase plays a role in protecting cells against nAg-mediated DNA damage and further growth arrest.

4. Discussion

The broad application of nAg to various commercial products and medical devices raises an issue about the safety of nAg in human health. Multiple lines of evidence from *in vitro* cell culture system suggest that nAg can trigger ROS generation possibly through mediating mitochondrial dysfunction and this causes membrane lipid peroxidation, DNA damage, and apoptosis (Ahamed et al., 2008; AshaRani et al., 2009). Several *in vivo* reports demonstrated the systemic distribution and toxicity of nAg in animals. nAg administered by oral route distributed throughout the body of rats, including the liver, kidneys, brain, and lung (Loeschner et al., 2011; Tang et al., 2009). In particular, accumulation of nAg

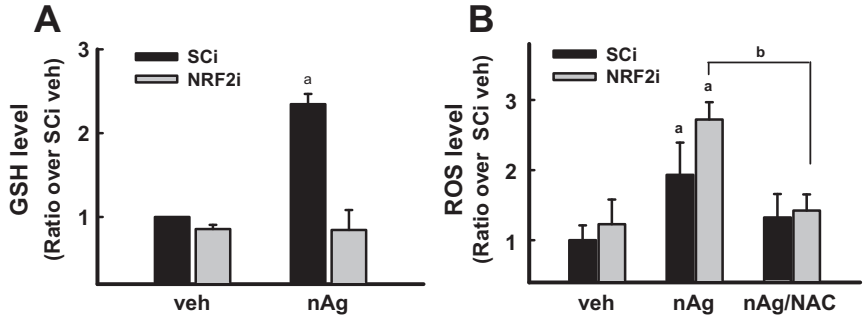

Fig. 5. GSH increase by nAg is impaired in NRF2i. (A) Cellular total GSH levels were determined following the treatment of SCi control and NRF2i with vehicle (veh, water) or nAg (60 μg/ml) for 48 h. (B) Levels of cellular ROS were monitored following vehicle or nAg (60 μg/ml) treatment for 48 h. NAC (5 mM) was added 6 h prior to nAg, and further co-incubated with nAg for 48 h. Values are means ± SD from three experiments. [a]$P < 0.05$ compared with vehicle-treated group. [b]$P < 0.05$ compared with nAg-treated NRF2i.

in the kidney was substantially high in rats. Together, it is of note that the accumulation was gender-specific and female rats showed a higher level of accumulation of nAg in the kidney than male rats (Kim et al., 2009, 2010). As a systemic toxicity, the liver toxicity has been reported: there were dose-dependent increases in liver damage markers, bile duct hyperplasia, fibrosis, and pigmentation following nAg over 125 mg/kg for 90 days. This raises a possibility that the kidney might be one of the major organs which can be affected by systemic action of nAg. In current study, the potential renal cell damage by nAg was examined in association with the function of NRF2 using human renal tubular epithelial cells. Due to increased DNA damage and G2/M cell cycle arrests, viable cell number was highly repressed by nAg in *NRF2* knockdown cells compared to SCi control. Distinct response to nAg was associated with GSH synthesis: nAg increase GSH synthesis in an NRF2-dpendent manner. This indicates that NRF2 functions to protect renal epithelial cells from nAg-mediated DNA damage and further cytotoxicity.

GSH is the primary ROS defense system in living organisms. Antioxidant function of GSH can be accounted by: (i) GSH directly interacts with ROS and reactive nitrogen species to eliminate these deleterious substances, (ii) GSH serves as a cofactor for GPX to remove hydrogen peroxide, and (iii) GSH involves in antioxidant recycling such as vitamin C regeneration (May et al., 1996). Because of its high concentration within the cell, GSH is considered as the primary direct ROS defense system that protects cells from oxidative damages (Anderson et al., 2004; Habib et al., 2007). Pharmacological depletion of GSH results in ROS increase, apoptotic response, and sensitization to oxidizing stimuli (Rahman et al., 2005). Similarly, severe oxidative stress can accumulate GSSG, which is an oxidized form of GSH, and GSSG itself can trigger

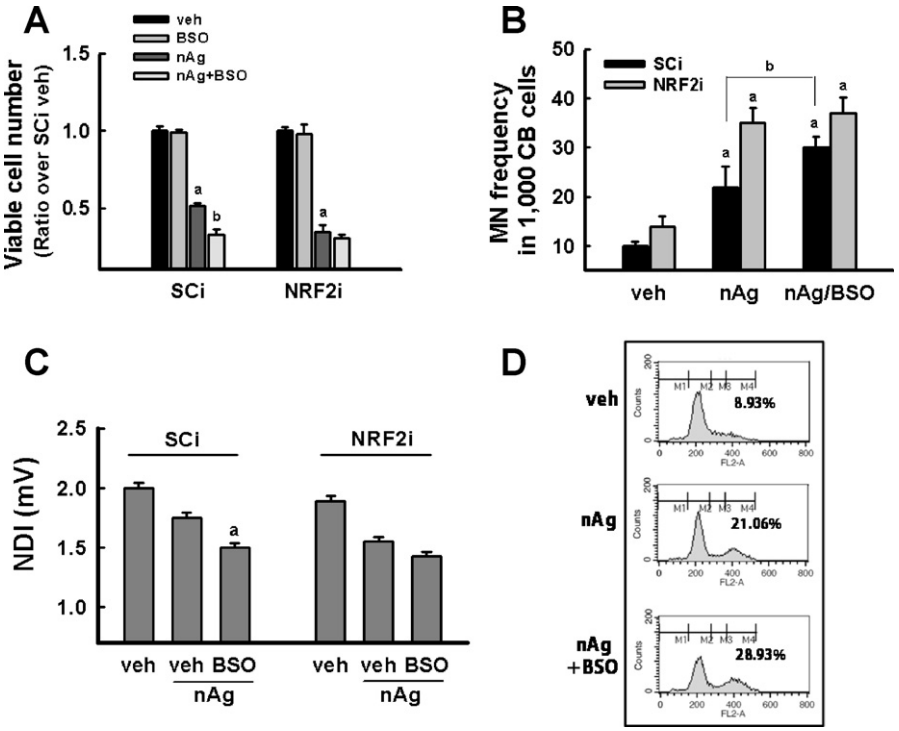

Fig. 6. nAg-mediated DNA damage and growth arrest are intensified by GSH depletion. (A) Viable cell number was determined by the MTT assay in SCi and NRF2i following treatment with vehicle (veh, water) or nAg (60 μg/ml) for 48 h. BSO (10 μM), a GSH depleting agent, was pre-incubated 6 h prior to nAg, and further co-incubated for 48 h. Values are means ± SD from three experiments. [a]$P < 0.05$ compared with each vehicle-treated group. [b]$P < 0.05$ compared with each nAg-treated group. (B) Levels of DNA damage measured by MN frequency were analyzed in SCi and NRF2i following nAg (60 μg/ml) for 48 h. Values are means ± SD from three experiments. [a]$P < 0.05$ compared with each vehicle-treated group. [b]$P < 0.05$ compared with each nAg alone-treated group. (C) The NDI values were determined in SCi and NRF2i following nAg (60 μg/ml) treatment for 48 h. Values are means ± SD from three experiments. [a]$P < 0.05$ compared with each nAg alone group. (D) Cell cycle distribution was analyzed following nAg (60 μg/ml) plus BSO for 48 h in nonspecific SCi control cells. Values are percentages of cells in G2/M phase.

apoptotic signaling by inhibiting mitochondrial function (Pias and Aw, 2002). These indicate that preservation of GSH is important to maintain cellular redox balance and normal cell physiology. GSH is synthesized in a two-step reaction catalyzed by the enzymes GCL and GSS. GCL catalyzes the first and rate-limiting step, forming γ-glutamylcysteine from glutamate and cysteine. The second step is catalyzed by GSS and adds a glycine to form GSH. GCL is a heterodimeric enzyme composed of GCLC and GCLM (Cortes-Wanstreet et al., 2009). The human *GCLC* and *GCLM* promoters contain multiple functional AREs, and these involve in the regulation of the basal and inducible expression of these genes (Erickson et al., 2002; Mulcahy and Gipp, 1995). Human *GSS* also contains ARE and is regulated by NRF2 signaling (Lee et al., 2005). These explain how NRF2 controls GSH level, while additional mechanisms aid the maintenance of GSH by NRF2. NRF2 controls expression of cysteine/glutamate exchange transporter (xCT) as well (Sasaki et al., 2002). Since this transporter regulates the influx of cysteine, which is a resource of GSH, NRF2 activation can contribute to GSH biosynthesis. Furthermore, GSH reductase (GSR), a reductive recycling enzyme of GSH, and radical scavenging GPX are NRF2-target genes in many types of cells (Hayes et al., 2010; Kwak and Kensler, 2010). Taken together, NRF2 is the critical factor to preserve cellular GSH level in response to environmental stress. In our study, nAg exposure evokes higher levels of DNA damage and growth arrest in NRF2 knockdown renal epithelial cells (NRF2i), and this is associated with GSH levels: (i) treatment of NRF2i cells with NAC, a GSH precursor, attenuates nAg-mediated DNA damage and growth arrest, (ii) GSH depletion in control cells intensifies nAg-mediated DNA damage and growth arrest, and (iii) nAg treatment activates NRF2 signaling and increases the expression of GCLC and GCLM, leading to GSH level increase; however due to an impaired inducibility, nAg cannot increase GSH level in NRF2i.

Cells bearing severe DNA damage halt the growth and proceed to apoptosis. These events can be beneficial to the whole organism by restricting genetic instability and preventing unintentional mutations. DNA damage signal is first transduced by ATM (Ataxia telangiectasia mutated) and ATR (Ataxia- and Rad-related) kinases to diverse signal transduction pathways for growth arrest (Niida and Nakanishi, 2006; Sorensen and Syljuasen, 2011). G2 phase is the period for the repair and restoration of damaged DNA, therefore, impairment of G2 checkpoint causes the abnormality of chromosome segregation and loss of gene information. For the transition from G2 phase to M phase, CDC2 and Cyclin B complex is required, and diverse signaling cascades can inhibit CDC2 activity as a checkpoint mechanism (Hu and Moscinski, 2011; Sorensen and Syljuasen, 2011). First, upon DNA damage, checkpoint kinase WEE1 phosphorylates CDC2 at Tyr15 and Thr14 and consequently inactivates CDC2 for G2-M progression. Phospho-CDC2 is dephosphorylated by CDC25C, which in turn can promote cell cycle progression. While, CDC25C can be inactivated by phosphorylation through the ATM/ATR-CHK1 signaling. Second, G2/M checkpoint can be regulated by p53 signaling as well (Niida and Nakanishi, 2006; Taylor and Stark, 2001). The kinase activity of CDC2 is regulated by its interaction with CDK inhibitor (CDKI) p21. The expression of p21 is up-regulated by p53; therefore, p53 plays a significant role in cell cycle arrest at G2/M as well as G1 phase. In addition, p53 is known to suppress the expression of Cyclin B (Taylor et al., 1999). Our results show that an enhanced DNA damage signal by nAg in NRF2 knockdown cells activates the components for G2/M checkpoint (summarized in Fig. 7). First, nAg increased levels of phospho-CDC2 (Tyr15) in both SCi and NRF2i, while the increase fold was greater in NRF2i than that in SCi. This suggests that DNA damage by nAg may activate WEE1 signaling for G2/M arrest. Second, nAg elevated phosphorylated CDC25C (Ser216) level, indicating that a greater accumulation of phospho-CDC2 in NRF2i can be related to the inactivation of CDC25C. Third,

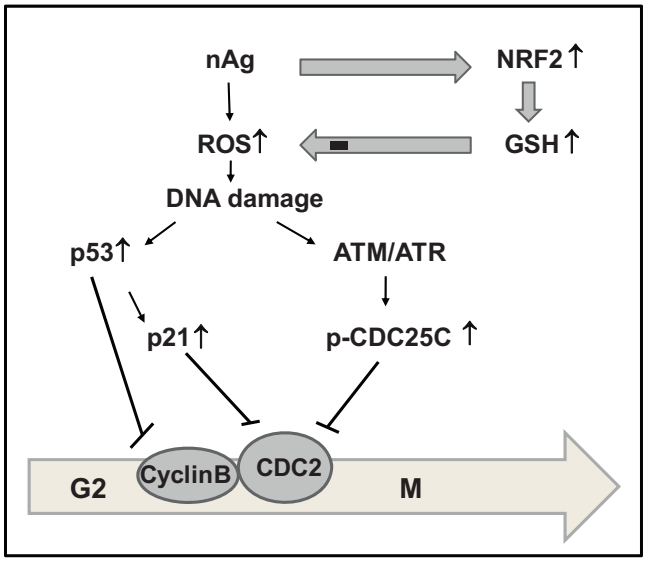

Fig. 7. The schematic mechanism of nAg-mediated G2/M arrest and the role of NRF2-GSH signaling. DNA damage by nAg activates the G2/M checkpoint through the inhibition of CDC25C and the activation of p53 signaling. Meanwhile, ROS-NRF2-GSH loop can protect renal epithelial cells from nAg-mediated G2/M arrest and further oxidative damage.

nAg induce p53-dependent checkpoint pathway: nAg elevated p53 protein level to a greater extent in NRF2i and accordantly, p21 level was highly elevated in these cells. Increased p21 may contribute to CDC2 inhibition for G2/M arrest together with WEE1/CDC25C pathways. In addition, elevated p53 appears to contribute to Cyclin B repression although there was no observable difference between SCi and NRF2i. Furthermore, we observed the elevation in p27 and Cyclin E1, and the reduction in CDK1 in NRF2i cells. These suggest that nAg can mediate G1/S arrest signaling, however, a cell cycle distribution analysis showed that G2/M arrest is predominant in nAg cytotoxicity. ROS-mediated cell cycle arrest and the involvement of NRF2 have been demonstrated in several studies. A report by Reddy et al. (2008) has demonstrated that the decrease in GSH synthesis by NRF2 function restriction causes DNA lesions and cell cycle arrest at G2/M phase. In our HK-2 cells, *NRF2* knockdown itself elevates p-CDC25C and p53 levels, although cell cycle distribution was not altered yet (Fig. 3A and B). However, nAg incubation in NRF2 inhibited cells appears to accelerate these changes to cause G2/M checkpoint activation. Recent several reports also demonstrated that nAg suppress the progression of cell cycle in lung epithelial and fibroblast cells, Jurkat T cell, and glioblastoma cells (AshaRani et al., 2009; Eom and Choi, 2010; Lee et al., 2011).

Taken together, the NRF2-GSH pathway is a sensitivity determination factor for nAg toxicity in renal epithelial cells. Suppression of NRF2 expression in these cells profoundly increased ROS production, DNA damage, and G2/M checkpoint activation. In the view of the protective role of NRF2 signaling in nAg cytotoxicity, dysfunction of NRF2 signaling, which might be derived from the genetic impairment or pathophysiological changes, may raise a concern about nAg safety in human health.

Conflict of interest statement

The authors declare that there are no conflicts of interest.

Acknowledgements

This work was supported by the National Research Foundation of Korea Grant (2011-0017977, 2011-0003619) funded by the

Korean government and the Research Fund, 2011 of The Catholic University of Korea.

References

Ahamed, M., Karns, M., Goodson, M., Rowe, J., Hussain, S.M., Schlager, J.J., Hong, Y., 2008. DNA damage response to different surface chemistry of silver nanoparticles in mammalian cells. Toxicology and Applied Pharmacology 233, 404–410.

Ahamed, M., Alsalhi, M.S., Siddiqui, M.K., 2010. Silver nanoparticle applications and human health. Clinica Chimica Acta 411, 1841–1848.

Anderson, M.F., Nilsson, M., Eriksson, P.S., Sims, N.R., 2004. Glutathione monoethyl ester provides neuroprotection in a rat model of stroke. Neuroscience Letters 354, 163–165.

AshaRani, P.V., Low Kah Mun, G., Hande, M.P., Valiyaveettil, S., 2009. Cytotoxicity and genotoxicity of silver nanoparticles in human cells. ACS Nano 3, 279–290.

Chaloupka, K., Malam, Y., Seifalian, A.M., 2010. Nanosilver as a new generation of nanoproduct in biomedical applications. Trends in Biotechnology 28, 580–588.

Churg, A., Stevens, B., Wright, J.L., 1998. Comparison of the uptake of fine and ultrafine TiO_2 in a tracheal explant system. American Journal of Physiology 274, L81–L86.

Cohen, M.S., Stern, J.M., Vanni, A.J., Kelley, R.S., Baumgart, E., Field, D., Libertino, J.A., Summerhayes, I.C., 2007. In vitro analysis of a nanocrystalline silver-coated surgical mesh. Surgical Infections (Larchmt) 8, 397–403.

Cortes-Wanstreet, M.M., Giedzinski, E., Limoli, C.L., Luderer, U., 2009. Overexpression of glutamate-cysteine ligase protects human COV434 granulosa tumour cells against oxidative and gamma-radiation-induced cell death. Mutagenesis 24, 211–224.

Donaldson, K., Stone, V., Seaton, A., MacNee, W., 2001. Ambient particle inhalation and the cardiovascular system: potential mechanisms. Environmental Health Perspectives 4 (Suppl. 109), 523–527.

Eastmond, D.A., Tucker, J.D., 1989. Identification of aneuploidy-inducing agents using cytokinesis-blocked human lymphocytes and an antikinetochore antibody. Environmental and Molecular Mutagenesis 13, 34–43.

Eom, H.J., Choi, J., 2010. p38 MAPK activation. DNA damage, cell cycle arrest and apoptosis as mechanisms of toxicity of silver nanoparticles in Jurkat T cells. Environmental Science and Technology 44, 8337–8342.

Erickson, A.M., Nevarea, Z., Gipp, J.J., Mulcahy, R.T., 2002. Identification of a variant antioxidant response element in the promoter of the human glutamate-cysteine ligase modifier subunit gene. Revision of the ARE consensus sequence. Journal of Biological Chemistry 277, 30730–30737.

Fenech, M., 2000. The in vitro micronucleus technique. Mutation Research 455, 81–95.

Fenech, M., 2007. Cytokinesis-block micronucleus cytome assay. Nature Protocols 2, 1084–1104.

Habib, G.M., Shi, Z.Z., Lieberman, M.W., 2007. Glutathione protects cells against arsenite-induced toxicity. Free Radical Biology and Medicine 42, 191–201.

Harvey, C.J., Thimmulappa, R.K., Singh, A., Blake, D.J., Ling, G., Wakabayashi, N., Fujii, J., Myers, A., Biswal, S., 2009. Nrf2-regulated glutathione recycling independent of biosynthesis is critical for cell survival during oxidative stress. Free Radical Biology and Medicine 46, 443–453.

Hayes, J.D., McMahon, M., Chowdhry, S., Dinkova-Kostova, A.T., 2010. Cancer chemoprevention mechanisms mediated through the Keap1-Nrf2 pathway. Antioxidants and Redox Signalling 13, 1713–1748.

Hu, X., Moscinski, L.C., 2011. Cdc2: a monopotent or pluripotent CDK? Cell Proliferation 44, 205–211.

Hwang, E.T., Lee, J.H., Chae, Y.J., Kim, Y.S., Kim, B.C., Sang, B.I., Gu, M.B., 2008. Analysis of the toxic mode of action of silver nanoparticles using stress-specific bioluminescent bacteria. Small 4, 746–750.

Kang, S.J., Kim, B.M., Lee, Y.J., Chung, H.W., 2008. Titanium dioxide nanoparticles trigger p53-mediated damage response in peripheral blood lymphocytes. Environmental and Molecular Mutagenesis 49, 399–405.

Kang, S.J., Ryoo, I.G., Lee, Y.J., Kwak, M.K., 2012. Role of the Nrf2-heme oxygenase-1 pathway in silver nanoparticle-mediated cytotoxicity. Toxicology and Applied Pharmacology 258, 89–98.

Kensler, T.W., Wakabayashi, N., Biswal, S., 2007. Cell survival responses to environmental stresses via the Keap1-Nrf2-ARE pathway. Annual Review of Pharmacology and Toxicology 47, 89–116.

Kim, W.Y., Kim, J., Park, J.D., Ryu, H.Y., Yu, I.J., 2009. Histological study of gender differences in accumulation of silver nanoparticles in kidneys of Fischer 344 rats. Journal of Toxicology and Environmental Health: Part A 72, 1279–1284.

Kim, Y.S., Song, M.Y., Park, J.D., Song, K.S., Ryu, H.R., Chung, Y.H., Chang, H.K., Lee, J.H., Oh, K.H., Kelman, B.J., Hwang, I.K., Yu, I.J., 2010. Subchronic oral toxicity of silver nanoparticles. Particle and Fibre Toxicology 7, 20.

Kim, T.H., Hur, E.G., Kang, S.J., Kim, J.A., Thapa, D., Lee, Y.M., Ku, S.K., Jung, Y., Kwak, M.K., 2011. NRF2 blockade suppresses colon tumor angiogenesis by inhibiting hypoxia-induced activation of HIF-1alpha. Cancer Research 71, 2260–2275.

Kirsch-Volders, M., Plas, G., Elhajouji, A., Lukamowicz, M., Gonzalez, L., Vande Loock, K., Decordier, I., 2011. The in vitro MN assay in 2011: origin and fate, biological significance, protocols, high throughput methodologies and toxicological relevance. Archives of Toxicology 85, 873–899.

Kobayashi, M., Yamamoto, M., 2005. Molecular mechanisms activating the Nrf2-Keap1 pathway of antioxidant gene regulation. Antioxidants and Redox Signalling 7, 385–394.

Kwak, M.K., Kensler, T.W., 2010. Targeting NRF2 signaling for cancer chemoprevention. Toxicology and Applied Pharmacology 244, 66–76.

Lee, T.D., Yang, H., Whang, J., Lu, S.C., 2005. Cloning and characterization of the human glutathione synthetase 5′-flanking region. Biochemical Journal 390, 521–528.

Lee, Y.S., Kim, D.W., Lee, Y.H., Oh, J.H., Yoon, S., Choi, M.S., Lee, S.K., Kim, J.W., Lee, K., Song, C.W., 2011. Silver nanoparticles induce apoptosis and G2/M arrest via PKCzeta-dependent signaling in A549 lung cells. Archives of Toxicology.

Liu, R., Choi, J., 2000. Age-associated decline in gamma-glutamylcysteine synthetase gene expression in rats. Free Radical Biology and Medicine 28, 566–574.

Loeschner, K., Hadrup, N., Qvortrup, K., Larsen, A., Gao, X., Vogel, U., Mortensen, A., Lam, H.R., Larsen, E.H., 2011. Distribution of silver in rats following 28 days of repeated oral exposure to silver nanoparticles or silver acetate. Particle and Fibre Toxicology 8, 18.

May, J.M., Qu, Z.C., Whitesell, R.R., Cobb, C.E., 1996. Ascorbate recycling in human erythrocytes: role of GSH in reducing dehydroascorbate. Free Radical Biology and Medicine 20, 543–551.

Mulcahy, R.T., Gipp, J.J., 1995. Identification of a putative antioxidant response element in the 5′-flanking region of the human gamma-glutamylcysteine synthetase heavy subunit gene. Biochemical and Biophysical Research Communications 209, 227–233.

Nemmar, A., Vanbilloen, H., Hoylaerts, M.F., Hoet, P.H., Verbruggen, A., Nemery, B., 2001. Passage of intratracheally instilled ultrafine particles from the lung into the systemic circulation in hamster. American Journal of Respiratory and Critical Care Medicine 164, 1665–1668.

Niida, H., Nakanishi, M., 2006. DNA damage checkpoints in mammals. Mutagenesis 21, 3–9.

Piao, M.J., Kang, K.A., Lee, I.K., Kim, H.S., Kim, S., Choi, J.Y., Choi, J., Hyun, J.W., 2011. Silver nanoparticles induce oxidative cell damage in human liver cells through inhibition of reduced glutathione and induction of mitochondria-involved apoptosis. Toxicology Letters 201, 92–100.

Pias, E.K., Aw, T.Y., 2002. Apoptosis in mitotic competent undifferentiated cells is induced by cellular redox imbalance independent of reactive oxygen species production. FASEB Journal 16, 781–790.

Rahman, I., Biswas, S.K., Jimenez, L.A., Torres, M., Forman, H.J., 2005. Glutathione, stress responses, and redox signaling in lung inflammation. Antioxidants and Redox Signalling 7, 42–59.

Reddy, N.M., Kleeberger, S.R., Bream, J.H., Fallon, P.G., Kensler, T.W., Yamamoto, M., Reddy, S.P., 2008. Genetic disruption of the Nrf2 compromises cell-cycle progression by impairing GSH-induced redox signaling. Oncogene 27, 5821–5832.

Samet, J.M., DeMarini, D.M., Malling, H.V., 2004. Biomedicine. Do airborne particles induce heritable mutations? Science 304, 971–972.

Sasaki, H., Sato, H., Kuriyama-Matsumura, K., Sato, K., Maebara, K., Wang, H., Tamba, M., Itoh, K., Yamamoto, M., Bannai, S., 2002. Electrophile response element-mediated induction of the cystine/glutamate exchange transporter gene expression. Journal of Biological Chemistry 277, 44765–44771.

Sondi, I., Salopek-Sondi, B., 2004. Silver nanoparticles as antimicrobial agent: a case study on *E. coli* as a model for Gram-negative bacteria. Journal of Colloid and Interface Science 275, 177–182.

Sorensen, C.S., Syljuasen, R.G., 2011. Safeguarding genome integrity: the checkpoint kinases ATR, CHK1 and WEE1 restrain CDK activity during normal DNA replication. Nucleic Acids Research 40, 477–486.

Tang, J., Xiong, L., Wang, S., Wang, J., Liu, L., Li, J., Yuan, F., Xi, T., 2009. Distribution, translocation and accumulation of silver nanoparticles in rats. Journal of Nanoscience and Nanotechnology 9, 4924–4932.

Taylor, W.R., Stark, G.R., 2001. Regulation of the G2/M transition by p53. Oncogene 20, 1803–1815.

Taylor, W.R., DePrimo, S.E., Agarwal, A., Agarwal, M.L., Schonthal, A.H., Katula, K.S., Stark, G.R., 1999. Mechanisms of G2 arrest in response to overexpression of p53. Molecular Biology of the Cell 10, 3607–3622.

Uejima, Y., Fukuchi, Y., Teramoto, S., Tabata, R., Orimo, H., 1993. Age changes in visceral content of glutathione in the senescence accelerated mouse (SAM). Mechanisms of Ageing and Development 67, 129–139.

Yoshimaru, T., Suzuki, Y., Inoue, T., Niide, O., Ra, C., 2006. Silver activates mast cells through reactive oxygen species production and a thiol-sensitive store-independent Ca2+ influx. Free Radical Biology and Medicine 40, 1949–1959.